The Mechanics of Diving Birds

Effect of Impact Forces as Birds Enter Water

Aschvin Chawan, Ravi Kappiyoor and Sunghwan Jung

5/10/2013

Abstract

Understanding the mechanics of birds diving into the ocean is a complex problem that has largely been unexplored. Many researchers have studied the energetics or diving depths of certain species, but none have addressed the impact forces, internal stresses, or fluid mechanics associated with this process. We attempt to simulate a simplified model of a diving bird. Our model consists of 2 small, hydrophobic spheres joined by an elastic polymer beam, similar in shape to a dumbbell. As this structure is released from a controlled height and impacts the water, we are able to see how the surface impact forces affect the dumbbell structure, causing the beam to buckle. We find that, while some birds have a very high flexural rigidity of their spine, allowing them to withstand the impact forces, other birds do not. Instead, they must make use of their neck muscles and geometrical advantages to minimize impact on the spine.

Introduction

Several species of birds dive into the ocean from high in the air to get their prey. As they dive, they can reach estimated velocities of up to 25 m s^{-1} just before impact with water. How do these birds withstand such high impact forces repeatedly over the course of their lives? What is the structural integrity of the bones required to perform this task? We aim to answer these questions herein.

Background

For our study, we have chosen 4 birds: the gannet, light mantled sooty albatross, brown pelican, and double crested cormorant. We begin this report with a brief introduction on relevant studies performed on these birds.

All of these birds exhibit plunge diving habits and must cope with similar stresses experienced by impact forces. An evolutionary advantage that all of these relatively large birds share is that their wings are more limber than the wings of smaller birds. Wing bones become proportionately thinner as length increases, making them less resistant to bending stresses. This allows for greater flexibility enabling these bones to withstand greater transient stresses during the diving process [1]. The ability to cope with greater stresses is also attributed to pneumatized skeletons. Pneumatic long bones have thinner cortices, reduced stiffness, and less resistance to bending when compared with size-matched apneumatic bones [2]. These bones are compact and exhibit more of the laminated and less of the fibrous texture than in other vertebrate classes [3]. With these common traits, we believe the stresses these birds develop are also related. One factor affecting impact forces is dive angle. This parameter has been shown to be a function of the perceived light refraction from the ocean's surface and visibility of the swimming prey [4, 5]. Not all of the relevant physiological data is available to be used in our model; instead, we can use allometric relations for certain diving variables to assume particular morphologies and characteristics [6]. A preferred bird tracker device to provide us with useful diving variables should include a submergence sensor, accelerometer, ECG (electrocardiogram) amplifier and electrode, batteries, communication port, and a thermistor [7], as shown in Figure 1.

Gannet

On sighting fish, the Northern gannet plummets down into the water from heights as high as 30 m. While diving, the bird can reach speeds up to 24 m s^{-1}. In the dive, the Northern gannet assumes a swept-back-wing posture, allowing for limited maneuverability. Immediately before impact the bird stretches its wings back for a spearhead entry. This positioning streamlines the body for entry to minimize impact forces [5]. After entry, the gannet has been known to exhibit U-shaped and V-shaped dives. The dive letters correspond to the path that the bird takes once under water. A V-shaped dive is typically at a shallower depth with a steeper entry and exit while a U-shaped dive involves the bird diving and rising back to the surface at a slower rate. The U-shaped dive can be shallow or deep [8]. It has been shown that this species does not streamline its body at a constant time-to-contact or at a constant height [5]. Researchers have found that the diving depths attained by the Northern gannet are not a function of body mass [9]. Among a species this relationship holds, but between species it breaks down. For the Northern gannet and Cape gannet, the maximum dive depths are inversely related to size [10]. The Northern gannet's dive speeds are similar to the maximum sustained swimming speeds of its pelagic prey [8]. These gannets are restricted to foraging mostly within the top 5 m of the water column, however their

absolute maximum diving depth approaches 13 m [11]. It is likely that these birds can only reach such depths by active underwater swimming [12]. For example, the Cape Gannet has been found to descend into the ocean at a rate of 2.87 m s^{-1} [13].

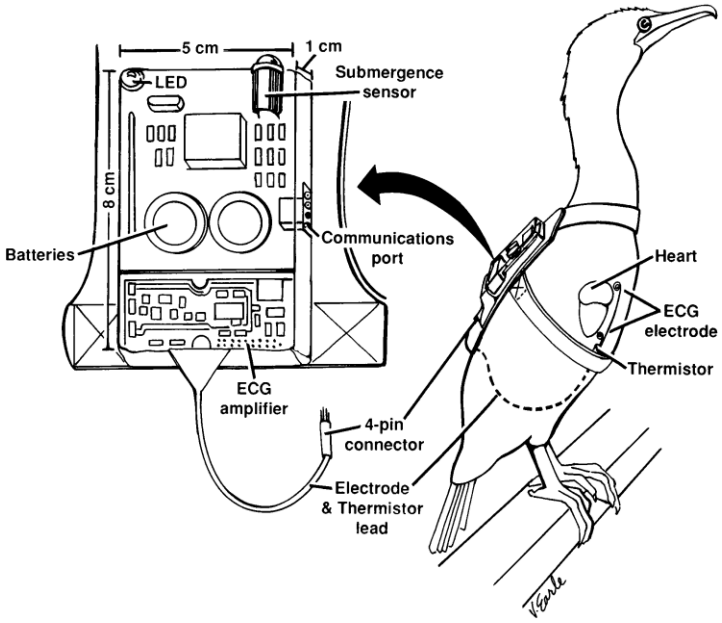

Figure 1: Bird Tracking Device Recommended for Double Crested Cormorant [7]

Light Mantled Sooty Albatross

Most recorded feeding methods of the light-mantled sooty albatross involve surface-seizing [14], supplemented by shallow plunges and dives from the surface [15]. Light mantled sooty albatrosses reach depths of up to 12 m while averaging 5 m. Among albatross species, the light mantled sooty albatross has a superior hydrodynamic design comprised of a slimmer body, longer wings, and pointed tails. It is also smaller than other albatrosses allowing it to travel underwater more efficiently. Albatrosses are less well-adapted to plunge-diving than gannets and most likely cannot penetrate the ocean's surface deeper than the gannet. This suggests that light-mantled sooty albatrosses, like the gannet, must also swim underwater to achieve recorded maximum diving depths [16].

Brown Pelican

While diving for food, brown pelicans are able to track their prey by adjusting their dive angle and height. This allows them to cope with the glare off of the water's surface [17]. Dive height may also affect the depth a plunge-diver can reach and may influence the number and diversity of potential prey [18]. Brown pelicans typically dive from 12-18 m above sea level. Dive angles are typically steep, greater than 60°, or flat, less than 30°. These differences can be attributed to the depth of the prey, the deeper the prey the steeper the dive [4].

Double Crested Cormorant

The diving characteristics of the double crested cormorant are not readily described in the literature. Few papers mention flock dynamics of these birds in response to prey aggregations in the ocean, but none focus on the factors that would assist this study. The cormorant dives at heights similar to the light mantled sooty albatross and its impact velocity is most closely related to this same bird. It has been found that large flocks pursue entire schools of fish, while smaller flocks hunt individual fish [19].

Methodology

Spine Properties *versus* Impact Velocity

As impact force is directly proportional to the square of the impact velocity, we hypothesize that the flexural rigidity of the spine, defined as the Young's modulus of the spine multiplied by the second moment of area of the spine, is also related to the square of the velocity. Unfortunately, testing this hypothesis is not straightforward as there is very little information regarding the Young's modulus and/or second moment of area of the spine of any of the aforementioned birds. As such, we take data that is readily available and make several assumptions.

There is little data available on the Young's modulus of the spine of the four birds that we wish to study. As such, we find the Young's modulus of the tibia of the light mantled sooty albatross and assume geometric similarity in order to calculate the Young's modulus of the spine of the same bird. To calculate the moment of inertia, we use data of average neck thickness of the bird multiplied by 0.25 in order to obtain a rough estimate of the average spine thickness. Using this information, we calculate the second moment of area of each bird.

In order to calculate the maximum force that the bird can withstand, we analyze a steady-state form of the Euler-Bernoulli beam equation:

$$EI\frac{\mathrm{d}^2v}{\mathrm{d}x^2}+Pv=0 \tag{1}$$

Here, E is the Young's modulus of the spine, I is the second moment of area of the spine, v is the deflection of the spine, x is the distance along the spine, and P is the force applied to the spine.

$$\frac{\mathrm{d}^2v}{\mathrm{d}x^2}+\frac{P}{EI}v=0 \tag{2}$$

$$\frac{\mathrm{d}^2v}{\mathrm{d}x^2}+k^2v=0 \tag{3}$$

Here, $k^2 = \frac{P}{EI}$. At this point, we have a Sturm-Liouville problem. If k^2 is either positive or zero, we obtain a trivial solution for *v*. As such, we require that k^2 is negative, which gives us the general solution:

$$v = C_1 \sin(kx) + C_2 \cos(kx) \tag{4}$$

We use the boundary condition that the angle of the beam at either end is zero to solve for C_1 and C_2.

$$v' = k\left(C_1 \cos(kx) - C_2 \sin(kx)\right) \tag{5}$$

$$v'(0) = kC_1 \cos(kx) = 0 \Rightarrow C_1 = 0 \tag{6}$$

$$v'(L) = -kC_2 \sin(kL) = 0 \Rightarrow C_2 = 0 \text{ or } kL = n\pi \tag{7}$$

Here, *n* is defined as any integer. To get a non-trivial solution for our initial differential equation, we require that:

$$k^2 = \frac{P}{EI} = \left(\frac{n\pi}{L}\right)^2 \tag{8}$$

$$P = EI\left(\frac{n\pi}{L}\right)^2 \tag{9}$$

The minimum force for buckling to occur can be found by setting *n* equal to 1, giving us:

$$P_{crit} = \frac{\pi^2 EI}{L^2} \tag{10}$$

We now relate this to the force experienced by the bird as it hits the water. Research shows that there is negligible deceleration as the bird hits the water, so the primary force on the bird is the drag force. This is calculated as:

$$P = \frac{1}{2}\rho C_D V^2 \tag{11}$$

Here, ρ is the density of the bird, C_D is the drag coefficient (which we assume to be 1 for this calculation). Setting (10) equal to (11) allows us to relate the flexural rigidity to the impact velocity.

$$EI = \frac{\rho L^2}{2\pi^2} V^2 \tag{12}$$

This gives us an equation for a minimum flexural rigidity required for a given impact velocity.

Dumbbell Model

While a simple analysis of spine properties *versus* impact velocity will provide some insights into the mechanics of diving birds, the story remains incomplete. We also need a better understanding of possible buckling mechanisms. In order to do this, we construct a simple model consisting of two small, hydrophobic spheres combined by an elastic polymer beam, similar in structure to a dumbbell. One sphere represents the head of the bird, while the other sphere represents the body of the bird. The elastic polymer beam represents the spine of the bird. This structure is dropped vertically in such a manner that the "head" of the structure impacts the water surface and propagates the impact force through to the spine. Experiments have been performed that show buckling in the "spine" of this structure.

Non-Dimensionalized Equation

We use a mathematical model in order to determine, quantitatively, the values of the flexural rigidity and impact force that are required for this buckling phenomenon. We begin with the Euler-Bernoulli beam equation:

$$\rho A\frac{\partial^2 v}{\partial t^2}+EI\frac{\partial^4 v}{\partial x^4}=\frac{P}{L} \tag{13}$$

Here, ρ is the density of the bone, A is the cross-sectional area, E is the Young's modulus, I is the moment of inertia, v is the deflection of the spine, P is the impact force, x is the position along the spine, and L is the length of the spine. We begin by non-dimensionalizing this equation. We do this by introducing the non-dimensional variables $\bar{v}=v/\bar{X}$, $\bar{x}=x/\bar{X}$ and $\bar{t}=t/\bar{T}$, where $\bar{X}$ and $\bar{T}$ are some characteristic length and time scale of the system, respectively. This gives us:

$$\rho A\frac{\bar{X}}{\bar{T}^2}\frac{\partial^2 \bar{v}}{\partial \bar{t}^2}+EI\frac{1}{\bar{X}^3}\frac{\partial^4 \bar{v}}{\partial \bar{x}^4}=\frac{P}{L} \tag{14}$$

$$\rho A\bar{X}\frac{\partial^2 \bar{v}}{\partial \bar{t}^2}+EI\frac{\bar{T}^2}{\bar{X}^3}\frac{\partial^4 \bar{v}}{\partial \bar{x}^4}=\frac{P}{L}\bar{T}^2 \tag{15}$$

From (15), we pick a convenient $\bar{X}$ to be $\bar{X}=1\,\text{kg}/(\rho A)$. The factor of 1 kg is included to ensure that $\bar{X}$ has units of length. Plugging this into (15) gives us:

$$(1\,\text{kg})\frac{\partial^2 \bar{v}}{\partial \bar{t}^2}+EI\left(\frac{\rho A}{1\,\text{kg}}\right)^3\bar{T}^2\frac{\partial^4 \bar{v}}{\partial \bar{x}^4}=\frac{P}{L}\bar{T}^2 \tag{16}$$

We define $\bar{T}^2=(1\,\text{kg})^4/EI(\rho A)^3$. The factor of $(1\,\text{kg})^4$ is included to ensure that $\bar{T}$ has units of time. This gives:

$$(1\,\text{kg})\frac{\partial^2 \bar{v}}{\partial \bar{t}^2}+(1\,\text{kg})\frac{\partial^4 \bar{v}}{\partial \bar{x}^4}=\frac{P}{L}\frac{(1\,\text{kg})^4}{EI(\rho A)^3} \tag{17}$$

$$\frac{\partial^2 \overline{v}}{\partial \overline{t}^2} + \frac{\partial^4 \overline{v}}{\partial \overline{x}^4} = \frac{P}{L} \frac{(1\,\mathrm{kg})^3}{EI(\rho A)^3} \tag{18}$$

We now non-dimensionalize the right-hand side of the equation by introducing the variables $\overline{P} = P / \overline{F}$ and $\overline{L} = L / \overline{X}$. Using the previous definition of $\overline{X}$, this gives us:

$$\frac{\partial^2 \overline{v}}{\partial \overline{t}^2} + \frac{\partial^4 \overline{v}}{\partial \overline{x}^4} = \frac{\overline{F}}{\overline{L}} \frac{\overline{P}}{EI(\rho A)^2} \frac{(1\,\mathrm{kg})^2}{} \tag{19}$$

We now define $\overline{F} = EI(\rho A / 1\,\mathrm{kg})^2$ to give us a final non-dimensional equation.

$$\frac{\partial^2 \overline{v}}{\partial \overline{t}^2} + \frac{\partial^4 \overline{v}}{\partial \overline{x}^4} = \frac{\overline{P}}{\overline{L}} \tag{20}$$

For convenience, we will drop the bar on each of the variables with the understanding that, henceforth in this document, all variables represent their non-dimensionalized forms. We use the boundary condition that the deflection and the angle of deflection are both zero at either end of the beam, and the initial condition that *v* is zero everywhere along the beam.

Finite Element Analysis

We use finite element analysis to obtain a numerical solution to (20). To do so, we must first derive the weak form of the equation. This is done by multiplying by an arbitrary test function, $\phi(x)$, and integrating over the domain (i.e. from 0 to *L*). This gives us:

$$\int_0^L \frac{\partial^2 v}{\partial t^2} \phi(x)\mathrm{d}x + \int_0^L \frac{\partial^4 v}{\partial x^4} \phi(x)\mathrm{d}x = \int_0^L \frac{P}{L} \phi(x)\mathrm{d}x \tag{21}$$

We first focus our attention on the second term of the left-hand side and integrate by parts.

$$\int_0^L \frac{\partial^4 v}{\partial x^4} \phi(x)\mathrm{d}x = \frac{\partial^3 v}{\partial x^3} \phi \Big|_0^L - \int_0^L \frac{\partial^3 v}{\partial x^3} \frac{\mathrm{d}\phi}{\mathrm{d}x}\mathrm{d}x \tag{22}$$

$$\int_0^L \frac{\partial^4 v}{\partial x^4} \phi(x)\mathrm{d}x = \frac{\partial^3 v}{\partial x^3} \phi \Big|_0^L - \frac{\partial^2 v}{\partial x^2} \frac{\mathrm{d}\phi}{\mathrm{d}x} \Big|_0^L + \int_0^L \frac{\partial^2 v}{\partial x^2} \frac{\mathrm{d}^2\phi}{\mathrm{d}x^2}\mathrm{d}x \tag{23}$$

Plugging (23) back into (21), we get:

$$\int_0^L \frac{\partial^2 v}{\partial t^2} \phi(x)\mathrm{d}x + \int_0^L \frac{\partial^2 v}{\partial x^2} \frac{\mathrm{d}^2\phi}{\mathrm{d}x^2}\mathrm{d}x = \int_0^L \frac{P}{L} \phi(x)\mathrm{d}x - \frac{\partial^3 v}{\partial x^3} \phi \Big|_0^L + \frac{\partial^2 v}{\partial x^2} \frac{\mathrm{d}\phi}{\mathrm{d}x} \Big|_0^L \tag{24}$$

We now use separation of variables to discretize *v* as:

$$v = \sum_{i=1}^{N} d_i(t)\psi_i(x) \tag{25}$$

In principle, *N* needs to be infinite in order to get an exact result. In practice, we will choose an *N* that is very large.

In order to satisfy the boundary conditions at all times, we need to have:

$$\psi_i(0) = \frac{\mathrm{d}\psi_i}{\mathrm{d}x}(0) = \psi_i(L) = \frac{\mathrm{d}\psi_i}{\mathrm{d}x}(L) = 0 \tag{26}$$

Until now, we have not required anything of the test function ϕ; the preceding derivation works for any ϕ that is defined from 0 to *L*. We now require that it is parallel to the spatial component of *v*. That is:

$$\phi = \sum_{j=1}^{N} e_j \psi_j(x) \tag{27}$$

This requirement immediately takes care of the boundary terms in (24), which vanish. Plugging the discretized functions in gives:

$$\ddot{d}_i\, e_j \int_0^L \psi_i \psi_j \mathrm{d}x + d_i e_j \int_0^L \frac{\mathrm{d}^2\psi_i}{\mathrm{d}x^2}\frac{\mathrm{d}^2\psi_j}{\mathrm{d}x^2}\mathrm{d}x - \frac{P}{L} e_j \int_0^L \psi_j \mathrm{d}x = 0 \tag{28}$$

$$\left(\ddot{d}_i \int_0^L \psi_i \psi_j \mathrm{d}x + d_i \int_0^L \frac{\mathrm{d}^2\psi_i}{\mathrm{d}x^2}\frac{\mathrm{d}^2\psi_j}{\mathrm{d}x^2}\mathrm{d}x - \frac{P}{L}\int_0^L \psi_j \mathrm{d}x \right) e_j = 0 \tag{29}$$

Here, we are using Einstein's summation convention. (29) is an orthogonality condition. Since we have no requirements placed on e_j, this can only be true if the quantity inside the parenthesis is zero. Defining variables M_{ij}, K_{ij}, and F_j as:

$$M_{ij} = \int_0^L \psi_i \psi_j \mathrm{d}x = M_{ji} \tag{30}$$

$$K_{ij} = \int_0^L \frac{\mathrm{d}^2\psi_i}{\mathrm{d}x^2}\frac{\mathrm{d}^2\psi_j}{\mathrm{d}x^2}\mathrm{d}x = K_{ji} \tag{31}$$

$$F_j = \frac{P}{L}\int_0^L \psi_j \mathrm{d}x \tag{32}$$

We can now write (29) as a matrix equation:

$$M_{ij}\ddot{d}_j + K_{ij} d_j = F_i \tag{33}$$

Using Hermitian basis functions for ψ_i, we solve numerically for d_j at each time step.

Results & Discussion

Spine Properties *versus* Impact Velocity

Table 1 below provides the data used to calculate the properties of the spine. Impact velocity data was taken from the literature. Figure 2 shows the correlation.

	Light Mantled Albatross	Brown Pelican	Northern Gannet	Double Crested Cormorant
Velocity (m/s)	2.30E+01	1.90E+01	2.50E+01	1.80E+01
Neck Thickness (m)	1.34E-01	7.22E-02	1.22E-01	5.93E-02
Spine Radius (m)	3.35E-02	1.80E-02	3.05E-02	1.48E-02
Dive Height (m)	3.10E+01	1.80E+01	3.00E+01	1.70E+01
Weight (g)	3.10E+03	3.70E+03	2.90E+03	1.90E+03
Mass of Spine (g)	1.55E+00	1.85E+00	1.45E+00	9.50E-01
Elastic Modulus (Pa)	2.236E+07	2.236E+07	2.236E+07	2.236E+07
Moment of Inertia (m^4)	1.98E-06	1.66E-07	1.36E-06	7.56E-08
EI	4.42E+01	3.72E+00	3.05E+01	1.69E+00
Height (m)	3.50E-01	6.80E-01	3.80E-01	5.10E-01
Density (kg-m^-3)	1.26E+00	2.66E+00	1.30E+00	2.70E+00
Min EI	4.12E+00	2.25E+01	5.96E+00	1.15E+01

Table 1: Calculation of Flexural Rigidity

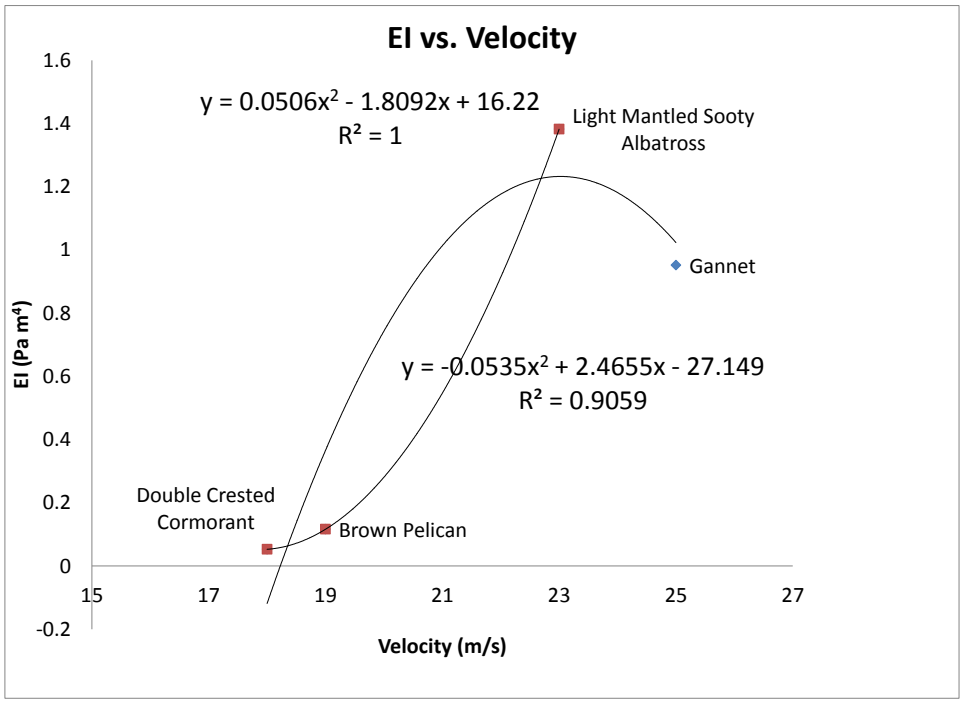

Figure 2: Flexural Rigidity *versus* Impact Velocity

We find that, as hypothesized, there does appear to be a strong quadratic correlation between the flexural rigidity and the impact velocity of the birds (R^2 = 0.9059). However, the coefficient on the quadratic term is negative. This does not make physical sense, as it would mean that, the flexural rigidity required to withstand the impact force at very high velocity is negligible. We note that, while the double crested cormorant, brown pelican, and light mantled albatross appear to follow an increasing flexural rigidity for an increasing velocity, the same is not true of the gannet. Indeed, if we remove the gannet from the above analysis, we find that the coefficient of the quadratic term becomes positive as indicated by the second fit applied to just the first three birds. We note that the R^2 value of the second fit is spurious; we have three data points and a quadratic function has three unknowns (the quadratic term, the linear term, and the constant). As such, R^2 will always equal 1. This indicates that either: (a) the gannet is doing something special that allows it to get away with less flexural rigidity in its spine, or (b) our approximation for the Young's modulus and second moment of area is incorrect. Unfortunately, as we do not have the ability to test the bones of any of these birds ourselves to determine the mechanical properties, we are unsure as to which of these possibilities holds true.

We take a closer look at the minimum required flexural rigidity of these birds in order to provide a better insight. From the data presented in Table 1, we find that only two of the four birds studied have a flexural rigidity higher than the theoretical minimum required. The other two birds are significantly lower. Upon closer inspection, we find that the two birds that have very low flexural rigidity as compared to the minimum theoretically required have longer necks than the other two birds. We hypothesize that, due to the increased length of the neck, the brown pelican and double crested cormorant use more neck musculature to absorb the impact of hitting the water, rather than the spine.

Unfortunately, the two approximate models used in this calculation yield different – and contradictory – results. Comparing the impact velocity to the flexural rigidity gave us the result that the gannet is doing something special. However, comparing the minimum theoretically required flexural rigidity to that found in the bird, we find that it is not the gannet, but the brown pelican and double crested cormorant that are doing something special. This is likely due to the inaccuracy of the assumptions we have made in order to get the data, and due to a very small sample size. In order to achieve a more complete understanding, then, more precise tests will have to be performed on a greater variety of birds.

Dumbbell Model

We now focus attention on the dumbbell model. Figure 3 shows the value of P that was used for the calculation as a function of time. We assumed a parabolic nature for P as the force will be minimal at first, increase as the dumbbell hits the water surface, and then decrease as the beam bounces back. L was assumed to be 10, and N was set to 1000.

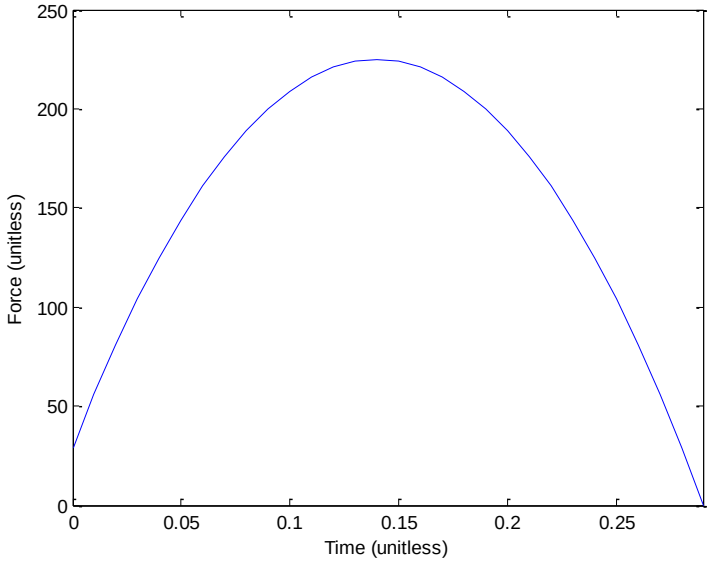

Figure 3: Impact Force *versus* Time

Using these values, we numerically calculate the deflection of the beam as time increases. In Figure 4, we show the deflection of the beam after 30 seconds from initial impact.

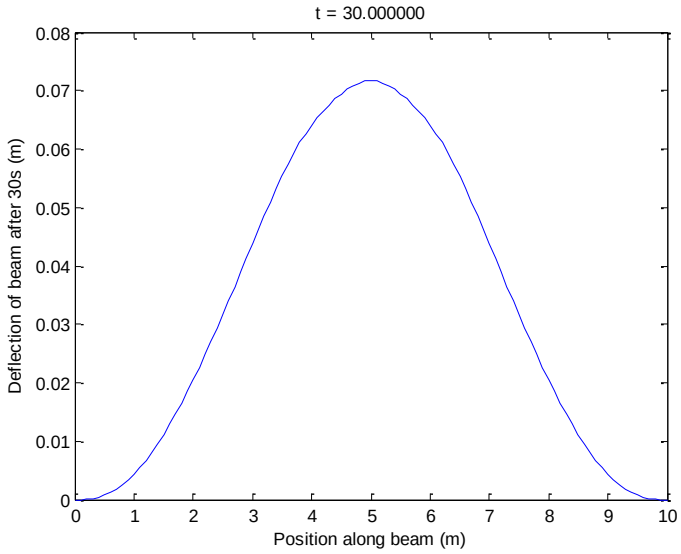

Figure 4: Deflection of Beam *versus* Position Along Beam

Conclusions & Future Work

Our results from the model provide contradictory results. This is primarily due to the assumptions made regarding the shape and strength of the spine of each bird. As such, there remains ample room for

future work on this topic. In order to get a better understanding of the effect of impact velocity on the required material properties of the spine, we would need to get more accurate data for the mechanical properties of the spines as well as finding data for more birds. This would provide insight as to the specific properties of bird impact. Further, the results of the model above need to be validated with experiments that have been performed. Currently, we have qualitative agreement, but do not have quantitative agreement. This indicates that the values used for the parameters are not exact, and need to be modified. Further, the model could be refined by changing the sphere that represents the head of the bird to a cone, simulating the existence of a beak; and further by adding a hook to this cone to simulate the hook of the beak.

References

1. Prange, H.D., J.F. Anderson, and H. Rahn, *Scaling of skeletal mass to body mass in birds and mammals.* American Naturalist, 1979: p. 103-122.
2. Fajardo, R., E. Hernandez, and P. O'Connor, *Postcranial skeletal pneumaticity: a case study in the use of quantitative microCT to assess vertebral structure in birds.* Journal of anatomy, 2007. **211**(1): p. 138-147.
3. Todd, R.B., *The cyclopaedia of anatomy and physiology*. Vol. 3. 1847: Sherwood.
4. Carl, R.A., *Age-class variation in foraging techniques by Brown Pelicans.* Condor, 1987: p. 525-533.
5. Lee, D.N. and P.E. Reddish, *Plummeting gannets: a paradigm of ecological optics.* Nature, 1981.
6. Halsey, L.G., P.J. Butler, and T.M. Blackburn, *A phylogenetic analysis of the allometry of diving.* The American Naturalist, 2006. **167**(2): p. 276-287.
7. Andrews, R., *Instrumentation for the remote monitoring of physiological and behavioral variables.* Journal of Applied Physiology, 1998. **85**(5): p. 1974-1981.
8. Garthe, S., S. Benvenuti, and W.A. Montevecchi, *Pursuit plunging by northern gannets (Sula bassana)" feeding on capelin (Mallotus villosus)".* Proceedings of the Royal Society of London. Series B: Biological Sciences, 2000. **267**(1454): p. 1717-1722.
9. Birt-Friesen, V., et al., *Activity-specific metabolic rates of free-living northern gannets and other seabirds.* Ecology, 1989: p. 357-367.
10. Brierley, A.S. and P.G. Fernandes, *Diving depths of northern gannets: acoustic observations of Sula bassana from an autonomous underwater vehicle.* The Auk, 2001. **118**(2): p. 529-534.
11. Adams, N. and C. Walter, *Maximum diving depths of Cape Gannets.* The Condor, 1993. **95**(3): p. 734-736.
12. Nelson, J.B., *The sulidae*. 1978: Oxford University Press.
13. Ropert-Coudert, Y., et al., *Between air and water: the plunge dive of the Cape Gannet Morus capensis.* Ibis, 2004. **146**(2): p. 281-290.
14. Harper, P., *Feeding behaviour and other notes on 20 species of Procellariiformes at sea.* Notornis, 1987. **34**(3): p. 169-192.
15. Milledge, D., *One year's observations of seabirds in continental shelf waters off Sydney.* Corella, 1977. **1**: p. 1-12.
16. Prince, P., N. Huin, and H. Weimerskirch, *Diving depths of albatrosses.* Antarctic Science, 1994. **6**(03): p. 353-354.
17. Sustare, B., *Physics of light: an introduction for light-minded ethologists.* The behavioral significance of color (EH Burtt, Jr., ed.). Garland STPM Press, New York, 1979: p. 3-27.
18. Dunn, E.K., *Effect of age on the fishing ability of Sandwich Terns Sterna sandvicensis.* Ibis, 1972. **114**(3): p. 360-366.

19. Bartholomew, G.A., *The fishing activities of double-crested cormorants on San Francisco Bay.* The Condor, 1942. **44**(1): p. 13-21.